Available online at www.sciencedirect.com
ScienceDirect
Acta Materialia 57 (2009) 5898–5913
Acta MATERIALIA
www.elsevier.com/locate/actamat

Alloys-By-Design: Application to nickel-based single crystal superalloys

R.C. Reed *, T. Tao, N. Warnken

Dept. of Metallurgy and Materials, University of Birmingham, Edgbaston B15 2TT, UK

Received 21 May 2009; received in revised form 5 August 2009; accepted 6 August 2009
Available online 4 September 2009

Abstract

Design rules are proposed by which the compositions of nickel-based single crystal superalloys can be chosen systematically, using models for the most important characteristics: creep resistance, microstructural stability, castability, density and cost. Application of the rules allows the very large compositional space to be reduced to just a few ideal compositions, which are likely to be close to the optimal ones. The procedures have the potential to remove much of the traditional reliance placed upon empiricism and trial-and-error-based testing. It appears that trade-offs must be accepted, however; for example, the most creep-resistant alloys are more dense, more costly and more inherently susceptible to casting-related defects such as freckles during processing. Compositions suitable for both jet propulsion and land-based applications are proposed, for future experimental testing.

Keywords: Nickel-based single crystal superalloys; Design of; Alloy compositions; Creep; Microstructural stability

1. Introduction

The nickel-based superalloys are remarkable for their resistance to mechanical and chemical degradation at temperatures up to 1000 °C and beyond [1,2]. Consider the most popular single crystal superalloys, which find application in a range of jet engines, land-based turbines and compression/pumping systems. Their chemical compositions [3] (see Table 1) confirm that a significant number of elements are added to nickel, e.g. Al, Ti and Ta to impart strengthening via the $Ni_3(Al, Ti, Ta)$ phase which is known as γ', Re, W and Mo to improve creep resistance, and Al, Cr and Co to impart resistance to oxidation, corrosion and sulphidation. There are few, if any, structural alloys which have this degree of compositional complexity.

It follows from these considerations that these alloys are unlikely to have been optimized as yet, and therefore that there are improved compositions – waiting to be discovered or perhaps designed – which are likely to be superior to those currently available. This can be confirmed by the following thought experiment. Table 1 indicates that at least eight alloying elements or more may be added, with concentrations needing to be chosen to an accuracy of at least 1.0 wt.% or probably better. Assuming for one moment that the optimum concentrations lie in the range 0–10 wt.%, empiricism alone would require approximately 10^8 alloys to be prepared, tested and ranked. Clearly, this is beyond the scope of any practical experimental programme of research. Instead, a degree of analysis and modelling is required if optimal alloys are to be isolated. It is probable that this argument applies to other classes of structural alloy, e.g. those based upon iron, aluminium or titanium.

As yet, there have been very few if any attempts to deal with this problem in a systematic way. Indeed, existing single crystal superalloys have been designed largely by empirical methods (see e.g. [4–8]). In principle, theoretical analysis and computer modelling tools might conceivably alter the prevailing emphasis on trial-and-error testing; obviously improvements in computational power, which are becoming available at modest cost, are likely to help in this regard. The present paper represents a first attempt to do this, for the case of the nickel-based single crystal superalloys. Any systematic design approach of the type proposed here must make use of suitable composition–microstructure–property relationships; for this reason, a

* Corresponding author. Tel.: +44 121 414 7080.
E-mail address: r.reed@bham.ac.uk (R.C. Reed).

1359-6454/$36.00 © 2009 Acta Materialia Inc. Published by Elsevier Ltd. All rights reserved.
doi:10.1016/j.actamat.2009.08.018

Table 1
Nominal chemical compositions (wt.%) of some selected nickel-based single crystal superalloys, and their associated densities [3]. The alloys appear in the approximate order of their appearance. Note the tendency to increased density, particularly due to rhenium additions.

Alloy	Cr	Co	Mo	Re	W	Al	Ti	Ta	Ni	Density (g/cm^3)
Nasair 100	9	–	1	–	10.5	5.75	1.2	3.3	Bal	8.54
CMSX-2	8	4.6	0.6	–	8	5.6	1	6	Bal	8.60
CMSX-6	9.8	5	3	–	–	4.8	4.7	2	Bal	7.98
PWA1480	10	5	–	–	4	5	1.5	12	Bal	8.70
SRR99	8	5	–	–	10	5.5	2.2	3	Bal	8.56
RR2000	10	15	3	–	–	5.5	4	–	Bal	7.87
Rene N4	9	8	2	–	6	3.7	4.2	4	Bal	8.56
AMI	7.8	6.5	2	–	5.7	5.2	1.1	7.9	Bal	8.60
AM3	8	5.5	2.25	–	5	6	2	3.5	Bal	8.25
TMS-6	9.2	–	–	–	8.7	5.3	–	10.4	Bal	8.90
TMS-12	6.6	–	–	–	12.8	5.2	–	7.7	Bal	9.07
CMSX-4	6.5	9	0.6	3	6	5.6	1	6.5	Bal	8.70
PWA1484	5	10	2	3	5	5.6	–	8.7	Bal	8.95
Rene N5	7	8	2	3	5	6.2	–	7	Bal	8.70
MC2	8	5	2	–	8	5	1.5	6	Bal	8.63
TMS-82+	4.9	7.8	1.9	2.4	8.7	5.3	0.5	6	Bal	8.93
CMSX-lfl	2	3	0.4	6	5	5.7	0.2	8	Bal	9.05
Rene N6	4.2	12.5	1.4	5.4	6	5.75	–	7.2	Bal	8.97
TMS-75	3	12	2	5	6	6	–	6	Bal	8.89

new theory for the composition-dependence of creep deformation in these materials is proposed. The methods are used to propose new versions of these alloys by considering the compositional space available; modelling methods are used to isolate compositions within it which are likely to be close to the optimal ones. Typical compositions are presented for future experimental confirmation of their properties.

2. Background

The single-crystal superalloys are used to fabricate the turbine blades which lie in the hot section of the turbine, immediately after the combustor arrangement [9] (see Fig. 1). Their role is to extract kinetic energy from the hot gas stream, to turn the turbine discs and ultimately the shaft so that power can be transmitted. In practice, the turbine blades are prone to deformation by creep processes [10,11]; excessive lengthening must be avoided since it compromises the aerodynamic efficiency of the engine. The stress σ in the blades arises largely due to centrifugal forces due to the significant rotational speeds – the angular speed ω can be 10,000 rpm or more – being of order

$$\sigma = \int_{r_{\text{root}}}^{r_{\text{tip}}} \rho\omega^2 r\, dr = \frac{\rho\omega^2}{2}\left(r_{\text{tip}}^2 - r_{\text{root}}^2\right) \quad (1)$$

where ρ is the blade density. The radial positions of the blade tip and root are given by r_{tip} and r_{root} respectively. The stress at the blade root can be estimated. Taking a conservative estimate of 100 s^{-1} for ω, $\rho = 9000$ kg/m^3, the blade height as 10 cm and the mean blade radius to be 0.5 m, it is approximately

$$9000 \times (100 \times 2\pi)^2 \times (0.55^2 - 0.45^2)/2$$

or 180 MPa. One sees that performance depends also upon the density; since the creep strain rate of the superalloy scales with σ^n – where n is the power law exponent which can be 5 or 6, or even greater – the density of the alloy should be minimized for longer creep life. Unfortunately, the density of the single crystal superalloys is increased by alloying with heavy elements such as Re and W, so that the greater creep resistance then conferred is offset somewhat by a greater density (see Table 1).

Microstructural design is a key requisite if creep resistance is to be optimized, and several factors are known to be of importance. First, the fraction ϕ_p of the strengthening γ' phase should be large enough to offer severe restriction to the passage of dislocations whose action is most usually restricted to the γ matrix channels lying between the precipitates. One can see this in constitutive models for creep deformation rate $\dot{\epsilon}$ which have been proposed for these materials, e.g. [12]

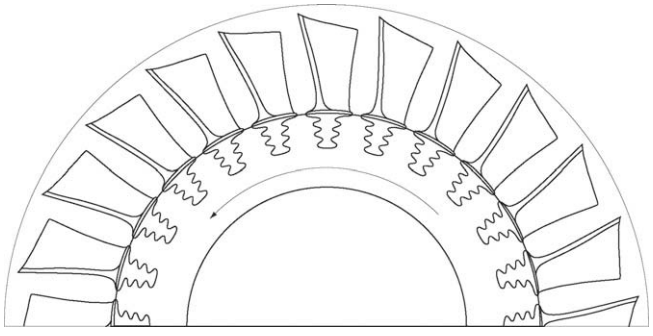

Fig. 1. Schematic illustration of turbine blades within a gas turbine engine, located on a turbine disc. Stresses are generated due to the action of centrifugal forces; creep extension occurs with the failure limit set by the dimensional tolerances with respect to the casing, which contains the hot gases.

$$\dot{\epsilon} = \rho_{\perp} f\{\phi_p\} c_j D_v \exp\left[\frac{(\bar{\sigma} - \sigma_r) b^2 \lambda_p}{\overline{M} kT}\right] \quad (2)$$

where $\rho_{\perp}$ is the density of creeping dislocations of Burgers vector b, λ_p is the spacing of the γ' particles, c_j is the density of jogs and $\overline{M}$ is the Taylor factor, determined for deformation expected in the cubic close-packed phase [12]. The term D_v is a volume diffusivity whose physical interpretation requires clarification; some clues about it will emerge in Section 3.1 of this paper. The function $f\{\phi_p\}$ can be taken to be of order unity.The macroscopic applied equivalent stress is denoted $\bar{\sigma}$ – it will contain a significant tensile component from the centrifugal loading – but, due to microstructural considerations, this is reduced by the sum of hardening terms σ_r, which includes an internal stress [12]; whilst some controversy exists about the origins of σ_r, most are agreed [10] that a first estimate of Gb/λ_p (where G is the shear modulus) is reasonable so that hardening is most potent when the γ' particles are closely spaced. Other constitutive equations which have been shown to model the creep deformation in these materials have a similar form [13]. In fact, as elegant experiments by Murakumo et al.[14] have shown, the optimal creep resistance is conferred when the γ' fraction is ~0.65 (see Fig.2), with the creep resistance being impaired at greater values due to an inability to control the cuboidal nature of the precipitation, so that the inversion occurs with γ' becoming the matrix phase. Second, adequate control of the γ/γ' lattice parameter misfit is required since otherwise excessive coarsening of the γ' structure occurs [15]. This is influenced by both preferential partitioning of elements between γ and γ' and by the manner in which the lattice parameters are then altered. Third, the microstructure should be stable with respect to the precipitation of topologically close-packed phases (TCPs), such as μ, σ and P [16,17]. TCP precipitation is known to be promoted by alloying with Cr and Mo; the PHACOMP [18] and M_d electron methods[19] have been shown to have predictive capability for the avoidance of TCP precipitation.

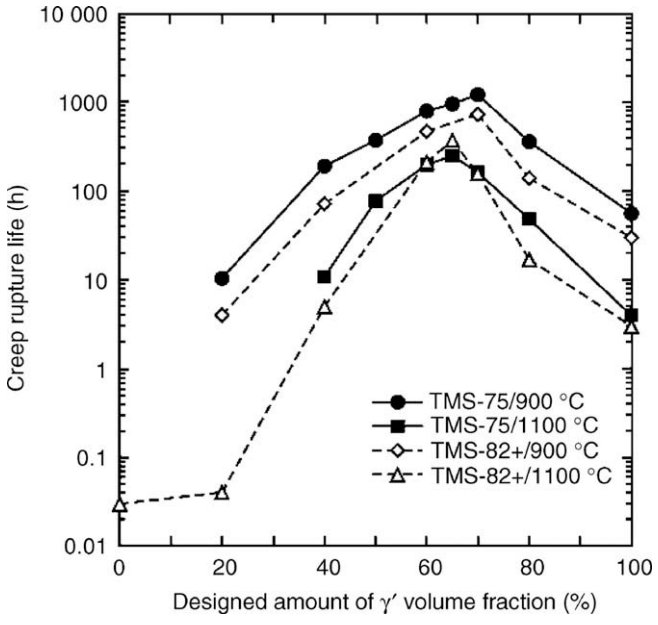

Fig. 2. Variation of creep rupture life for the single crystal superalloys TMS-75 and TMS-82+, measured for varying γ and γ' fractions of identical compositions [14].

Finally, the manufacturing by investment casting should be considered since it is well established that some grades of single crystal superalloy are easier to cast than others [3]. The chief difficulty is the occurrence of casting-related defects known as freckles, which are known to trigger the formation of stray grains which must be avoided [20]. Freckling occurs due to thermo-solutal driven flow on the scale of the mushy zone, caused by density inversion due to elemental partitioning between the liquid and the growing solid phase [21]. Thus, freckling is exacerbated by the partitioning of heavier elements such as Re and W to the solid; this is mitigated by partitioning of Ta to the liquid phase. Clearly, the availability of thermodynamic databanks coupled with estimates of the liquid densities would provide predictive estimates for freckling susceptibility. The costs of the elemental additions will also be an important consideration.

Fig. 3 summarizes the performance characteristics which are known to be important for the single crystal superalloys. These need to be accounted for in the alloy design process.

3. Procedures and models

In what follows, methods are presented by which the key performance characteristics of the single crystal superalloys can be estimated. Use will be made of various data [3] for the alloying elements added to the superalloys (see Fig. 4); included is information for the densities of the pure elements, their cost and the values estimated recently for the interdiffusion coefficient of each element with nickel [22]. As expected, a strong correlation exists with atomic number, with the values varying systematically with the position of the alloying element within the periodic table.

3.1. Estimation of creep resistance

No fundamental theory exists at present that allows the creep resistance of the superalloys to be estimated from an initial estimate of the chemical composition; probably this

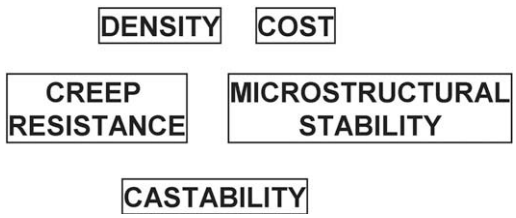

Fig. 3. Summary of the important characteristics of the single crystal superalloys.

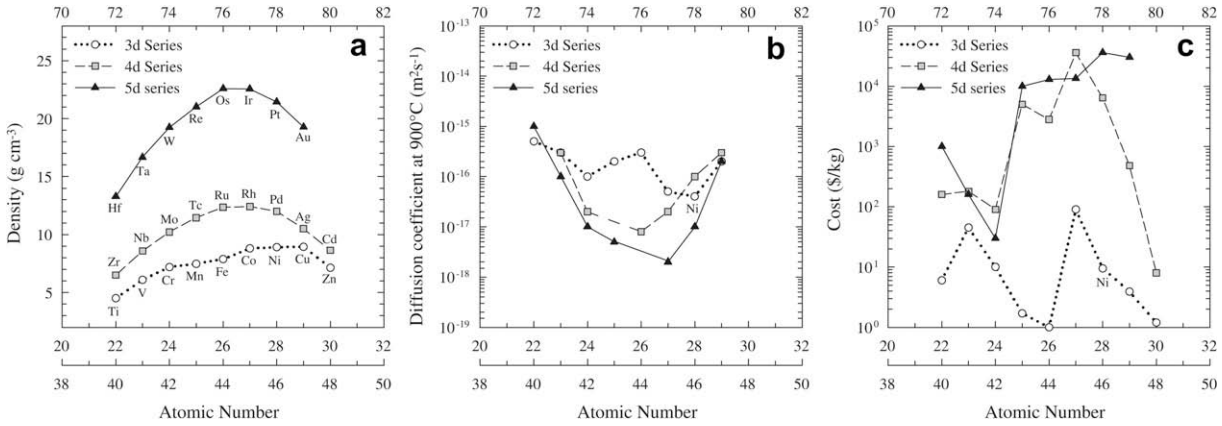

Fig. 4. Various data used for the calculations reported here [3].

is because the composition-dependence of the rate-controlling steps has until now remained ill-defined. Instead, use of regression analysis or neural networks has been common (e.g. [5]). However, recent theoretical work [22] using ab initio methods has shed light on the effect of the transition metals on the atomic-scale processes occurring on the nickel lattice, in particular the dependence of solute/vacancy exchange energies on the atomic number of the solute. This is relevant to high temperature properties such as creep deformation, for which a significant thermally activated component is expected; indeed, the modelling has been used to rationalize the strong correlation observed experimentally [23] between the interdiffusion coefficient $\widetilde{D}_i$ of a solute element i and its atomic number, as summarized in Fig. 4b. Solutes from the centre of the d-block exhibit the largest solute/vacancy exchange energies; for example, the solute/vacancy exchange energy for Re is about 170 kJ mol^{-1} [22] and the largest of those elements commonly added to the superalloys. These findings allow a first-order theory for the composition-dependence of creep deformation in this system to be proposed. Our basic premise is that the values of the activation energies controlling diffusional processes in these materials [22,23] are reasonable estimates for those controlling the rates of transport processes occurring as dislocations percolate through the microstructure.

One proceeds as follows. Consider the accumulation of creep strain due to the passage of dislocations, their migration occurring by a coupled climb/glide process which exhibits a strong (and rate-controlling) thermally activated component (see Fig. 5). The leading segment of the dislocation encounters a site density $n_{\mathrm{Re}}, n_{\mathrm{W}}, n_{\mathrm{Ta}}$, etc. of pinning atoms, the strength of which will vary from solute to solute; thus there is a characteristic time of escape, denoted $t_{\mathrm{Re}}, t_{\mathrm{W}}, t_{\mathrm{Ta}}$, etc., which must be overcome by thermal activation. These depend upon critical activation energies $Q_{\mathrm{Re}}, Q_{\mathrm{W}}, Q_{\mathrm{Ta}}$, etc., which are associated with the breaking away of each segment of the dislocation core from the solute atom. It follows that the effective time to circumvent a unit length of pinning atoms, denoted t_{eff}, is given by

$$t_{\mathrm{eff}} = n_{\mathrm{Re}} t_{\mathrm{Re}} + n_{\mathrm{W}} t_{\mathrm{W}} + n_{\mathrm{Ta}} t_{\mathrm{Ta}} + \cdots + n_i t_i \qquad (3)$$

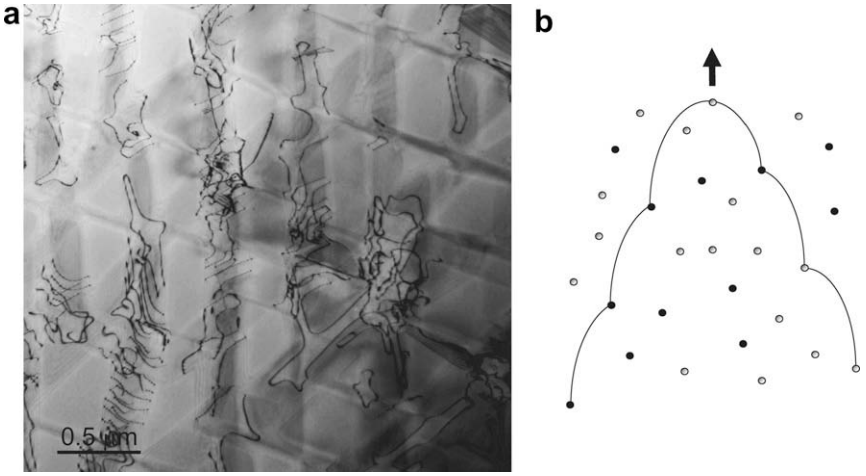

Fig. 5. (a) Transmission electron micrograph (foil normal {1 1 1}) of the CMSX-4 single crystal superalloy, deformed to 0.04% creep strain in 1890 h at 750 °C and 450 MPa; note that the deformation is restricted to the γ channels; (b) schematic illustration of the expansion of dislocation loop in the γ channel, controlled by interaction with pinning atoms of different types.

where

$$t_i \propto 1/\exp\left\{-\frac{Q_i}{RT}\right\} \tag{4}$$

where Q_i is the activation energy associated with the unpinning needed from the solute i. In the absence of better estimates, it is assumed that values of the interdiffusion coefficients $\widetilde{D}_i$ [22,23] (see Fig. 4) can be used as suitable proxies for Q_i; since the pre-exponential terms are found not to vary strongly with solute i [22], this amounts to assuming that $Q_i \simeq \widetilde{Q}_i$ where $\widetilde{Q}_i$ is the activation energy pertaining to the interdiffusion process, for which reasonable estimates are known [22,23]. These considerations suggest that a suitable merit index for creep resistance, denoted M_{creep}, is

$$M_{\text{creep}} = \sum_i x_i/\widetilde{D}_i \tag{5}$$

where x_i is the atom fraction of solute i present in the alloy and $\widetilde{D}_i$ is the appropriate interdiffusion coefficient (see Fig. 4). One would expect that the creep resistance scales with M_{creep} and those compositions with the greatest values to perform best. Note that, since the variation of $\widetilde{D}_i$ with atomic number depends largely upon differences in the activation energy (with the pre-exponential term rather invariant with it [22]), one is making use of an expected similarity of the atomic-scale processes controlling dislocation creep and those controlling vacancy-assisted diffusion.

Practical considerations in gas turbine engineering dictate that the time to 1% strain is an important quantity which needs to be maximized. Fig. 6a confirms that the proposed merit index compares favourably with published data for the time to 1% creep strain for a number of experimental single crystal superalloys [24–26] of various generations, which were tested at 900 °C/392 MPa – a good approximation for the conditions experienced by these materials in service. If the x_i's of Eq. (4) are evaluated from the predicted mole fractions in the γ phase at 900 °C – consistent with the methods introduced in Section 3.3 – then the values of M_{creep} are increased, due to the preferential partitioning of Re to γ. The agreement is somewhat improved, although for the purposes of the present work the mean compositions have been deemed sufficiently accurate.

The theory is further supported by the following. Fig. 4 indicates that the time to 1% strain at 900 °C/392 MPa is a few hundred hours, or of order 10^6 s. Assuming a characteristic distance – consistent with the periodicity of the γ/γ' microstructure – of about 1 μm, which is reasonable for these materials [3], then the rate controlling value of $\widetilde{D}_i$ is predicted to be 1×10^{-18} m^2 s^{-1}. This is not very different from the value for Re at 900 °C (see Fig. 4).

3.2. Estimation of density

The density of pure nickel under ambient conditions is 8907 kg m^{-3} [3], but alloying leads to densities of single crystal superalloys which are appreciably different from this value (see Table 1). A first estimate of the density of a new single crystal superalloy can be made from the values of the pure elements, provided that a rule of mixtures is assumed. It has been found that this procedure underestimates the true density by a factor of about 5%, due to the differing bonding characteristics which then prevail. Once this correction factor is accounted for, the density can be estimated accurately, to within 1%. Fig. 7 compares experimental data [3] for a number of single crystal superalloys (the compositions and densities are given in Table 1) with the predictions made in this way.

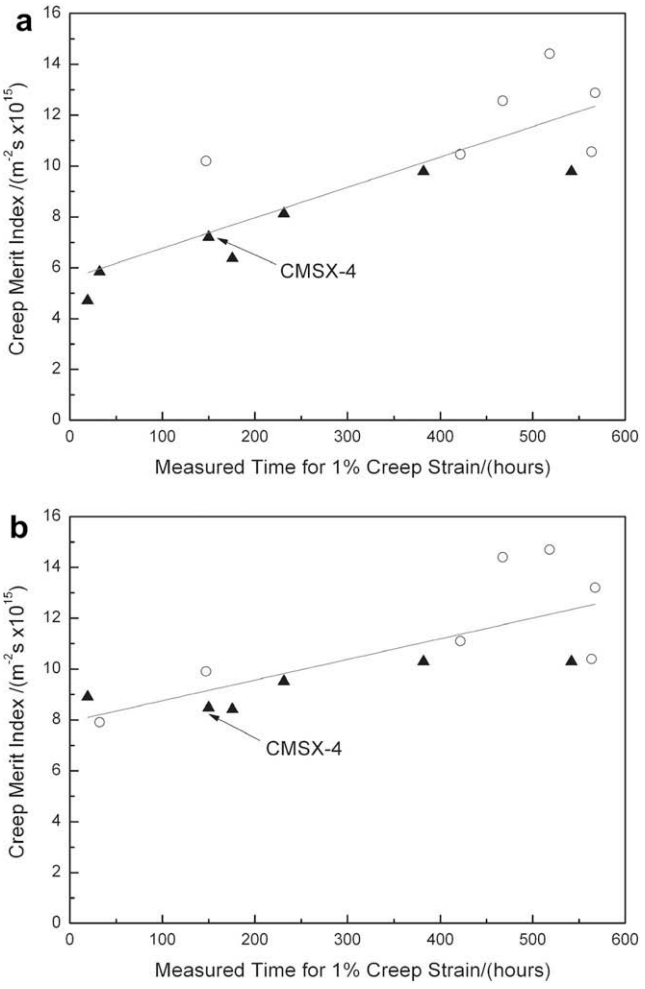

Fig. 6. Comparison of computed values of the merit index M_{creep} with measured values of the time to 1% strain (conditions 900 °C, 390 MPa) for various prototype nickel-based single crystal superalloys [24–26]: (a) assuming $\bar{x}_i$'s, the mean elemental compositions; and (b) assuming $x_i^{\gamma\prime}$'s, the mole fractions in γ at 900 °C computed using Thermo-calc. Note that the open circles correspond to Ru-containing superalloys.

3.3. Estimation of microstructural characteristics and stability

Three major microstructural characteristics known to influence the creep properties of the single crystal superal-

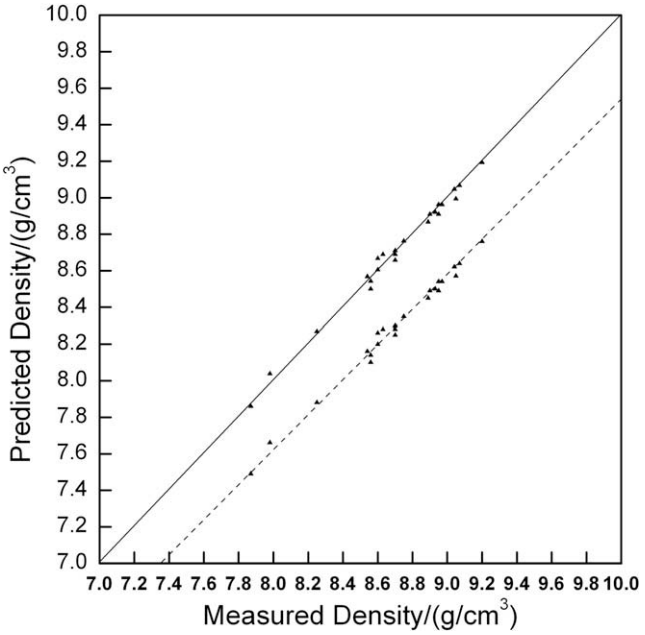

Fig. 7. Comparison of the measured densities of the single crystal superalloys given in Table 1, and those computed assuming densities of the pure elements, after application of a factor of 1.05 to increase the computed density. The dashed line indicates the best-fit line in the absence of the correction factor.

loys were estimated as a function of alloy chemistry: (i) the γ' fraction (see Fig. 2), (ii) the γ/γ' lattice misfit and (iii) the susceptibility to precipitation of TCP phases.

The Thermocalc software [27] and an underlying database of thermodynamic parameters for the nickel-based superalloys [28] were used to make predictions of multiphase, multicomponent equilibria in these systems. Calculations for the γ/γ' equilibria were made at 900 °C, close to the anticipated operating conditions of the alloys, thus allowing the compositions of both matrix and precipitate phase to be determined. Since the coherency of the γ/γ' interface is important and needs to be maintained, the lattice parameters of the two phases were estimated at 900 °C according to

$$a_\gamma = 3.559257 + 0.0000198T + \sum_i \Gamma_i^\gamma x_i \quad \text{Å} \tag{6a}$$

and

$$a_{\gamma'} = 3.552743 + 0.0000552T + \sum_i \Gamma_i^{\gamma'} x_i \quad \text{Å} \tag{6b}$$

where the x_i represent the mole fractions in the appropriate phase and the temperature T is given in kelvin. The terms Γ_i^γ and $\Gamma_i^{\gamma'}$ are Vegard coefficients; the values employed in the calculations are listed in Table 2. The lattice misfit δ was then defined as the difference between the lattice parameters divided by their average, in the usual way [3], with a negative misfit implying $a_{\gamma'} < a_\gamma$. Note that the Vegard parameters in the above expressions were estimated by Reed [3], through the consideration of lattice parameter changes seen in the binary Ni-X systems; their values correlate strongly with atomic number, elements at the centre of the d-block exhibiting the smallest values for any given phase. The remaining terms in the expressions were chosen to reproduce the lattice misfit of $+8 \times 10^{-4}$ and lattice parameters 3.623024 Å (for γ) and 3.625800 Å (for γ') which have been reported for the CMSX-4 single crystal superalloy at 900 °C [5].

Table 2
Values of the Vegard coefficients used in this study for the calculation of lattice misfit.

Values of Vegard coefficients (Å/atom frac)	Matrix phase Γ_i^γ	Precipitate phase $\Gamma_i^{\gamma'}$
Cr	0.110	−0.004
Co	0.020	−0.004
Re	0.441	0.262
W	0.444	0.194
Al	0.179	0.000
Ta	0.700	0.500

In the above, the possibility of precipitation of TCP phases is not accounted for. To do this, and in the absence of better electronic structure calculations, use has been made of simplified estimates of the energy levels expected (in eV) from elementary band theory [6,19]. These have been termed metal-d levels (denoted M_d) and have been found to correlate well with the electronegativity and the metallic radius. To estimate TCP susceptibility, one then works out the effective $\overline{M_d}$ level (in eV) from

$$\overline{M_d} = \sum_i \bar{x}_i M_{di} \tag{7}$$

where the $\bar{x}_i$ correspond to the mole fraction of i in the alloy and the values of M_{di} for the various i's from the d-block of transition metals are given in Fig. 8 (note for Al the appropriate value is 1.9 [6,19]). The higher the value of the stability number $\overline{M_d}$, the greater the probability of TCP formation. In a variant of the procedure, the concentration terms in the summation can be taken to be the predicted mole fractions in γ.

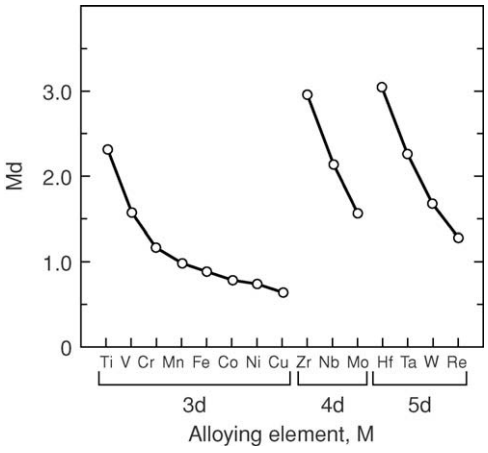

Fig. 8. Variation with atomic number of the M_d number, used for assessment of the susceptibility of the single crystal superalloys to TCP phases. Values taken from Refs. [6,19].

3.4. Estimation of cost

The cost of a prototype single crystal superalloy is determined provided that estimates are available for the costs of the raw elements employed. These are subject to the movements of metal markets. The values used in our calculations are given in Fig. 4; they are accurate as of the early part of 2009. Our estimates assume that processing costs are identical for all alloys, *i.e.* that the product yield is not affected by composition.

3.5. Estimation of castability

The castability is assumed to be controlled by the resistance to freckling; the freckle defect is promoted when the interdendritic liquid is sufficiently lightened by the partitioning of the heavier elements to the dendrite cores. In the first part of the work, we have assumed that the necessary density changes arise only from the partitioning of Re, W and Ta; since it is known that Re and W partition to the solid phase and Ta to the liquid phase, the following phenomenological equation is used to rank castability [29]

$$M_{\text{castability}} = w_{\text{Ta}}/(1.2w_{\text{Re}} + w_{\text{W}}) \quad (8)$$

where w_{Ta}, w_{Re} and w_{W} correspond to the mean weight fractions of Ta, Re and W respectively in the alloy. Note that castability is promoted when the merit index $M_{\text{castability}}$ is large. In Section 6, consideration is given to a more rigorous castability index which accounts for the changes in density which are expected during solidification; however, in the first part of the paper, Eq. (8) is deemed to be sufficiently accurate.

4. Results

To illustrate the power of our methods, calculations have been made in the Ni–Cr–Co–Re–W–Al–Ta system. In the first instance, the Cr concentration is taken to vary from 4 to 12 wt.%, the Co concentration from 0 to 10 wt.%, the Re concentration from 0 to 5 wt.%, the W concentration from 0 to 8 wt.%, the Al concentration from 4 to 7 wt.% and the Ta concentration from 4 to 8 wt.%. Calculations are carried out at a resolution of 1 wt.%; the compositional dataset then consists of a total of ~100,000 alloys. No effort has been made to account for the effects of Ti, Mo or Ru due the detrimental effects on oxidation resistance, corrosion and cost respectively. However, the methods can be adapted readily to account for the presence of these elements.

4.1. Histograms

In Fig. 9, data are plotted for various predicted characteristics of the ~100,000 alloys in the compositional space considered. The histograms help to confirm whether or not a good statistical spread in the properties is expected. A substantial variation in the properties is indeed predicted. For example, the relative density is estimated to vary from 8.0 to beyond 9.3, the γ' fraction at 900 °C from 0.05 to 0.90, the lattice misfit lies in the range $\pm 1 \times 10^{-2}$ and the stability number in the range 0.85–1.05 eV. The histogram for cost does not conform to a Gaussian distribution; this effect has been traced to the very strong biasing of the data by the Re concentration, due to this element's substantial price (see Fig. 4). The data for the merit index for creep indicate that a substantial variation in the creep performance is to be expected.

4.2. Trade-off diagrams

The data in Fig. 9 demand further interpretation, since it is unlikely to be the case that any one set of alloys will exhibit the very best properties in each category. It follows that trade-offs between the different characteristics need to be identified. To facilitate this, the concept of "trade-off" diagrams has been developed; for all alloys in the dataset, one property (e.g. density, cost, creep) is used as a criterion to sort the list of ~100,000 alloys into rank order. Since the other properties can then be determined, this allows correlations between the different properties to be identified.

Since creep resistance is of paramount importance, correlations with that are identified first. Fig. 10 illustrates trade-off diagrams for creep resistance against density, cost, stability and castability. Fig. 10a confirms a correlation of the creep resistance and density, with the more creep-resistant alloys tending to be more dense; however, for any given value of the creep merit index, a set of alloys with a considerable range of densities can be found, implying that there is room for manoeuvre. Fig. 10b confirms a correlation between creep resistance and cost, with the more creep-resistant ones costing more in general; however, once again it is possible to find adequate creep resistance at moderate cost. The plot against stability number $\overline{M_{\text{d}}}$ indicates that the most creep-resistant alloys are generally more prone to instability (see Fig. 10c). Finally, the plot against castability indicates that the very best creep resistance (implying significant quantities of Re and W) can be attained only at the expense of castability (see Fig. 10d).

It is possible to identify a number of further trade-off diagrams, but in the interests of brevity only the more revealing are presented here. In Fig. 11a, the plot of density against stability number $\overline{M_{\text{d}}}$ indicates no direct correlation, but alloys close to the median density exhibit a wider spread in predicted stability than those which are very dense or very light; it is significant that alloys which are light can nonetheless be prone to instability. No correlation at all was found between cost and density (see Fig. 11b); at any given density, both expensive and cheap alloys can be identified. Finally, the plot of cost against stability number $\overline{M_{\text{d}}}$ (see Fig. 11c) warrants consideration. The data for $\overline{M_{\text{d}}}$ fall into six vertical bands, each corresponding to a concentration of Re. Within each band, alloys which are most unstable (corresponding to large $\overline{M_{\text{d}}}$) are those with high concentrations of Ta and Al; those with low concentrations

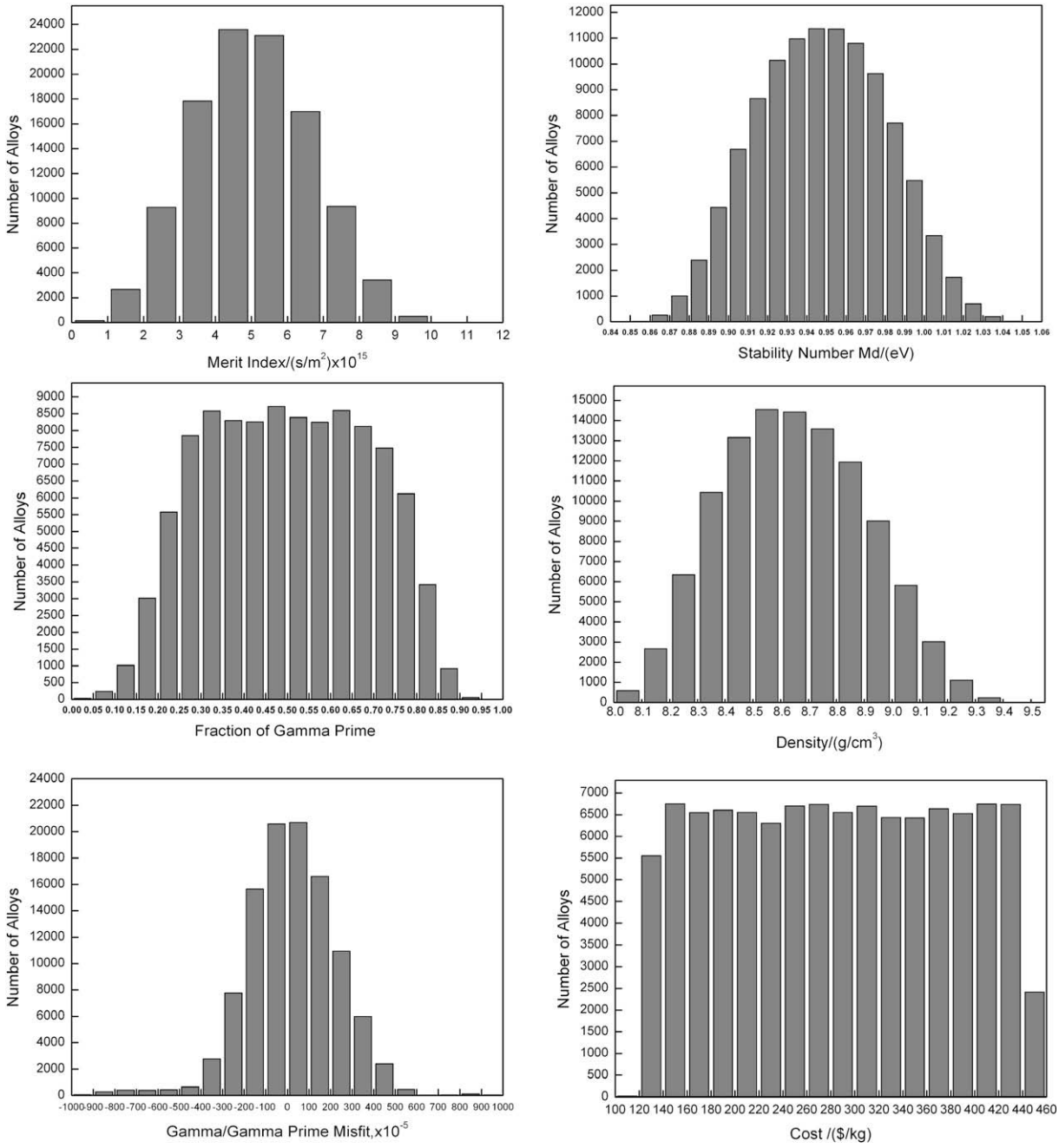

Fig. 9. Computed histograms for the alloys under consideration: (i) the creep merit index; (ii) fraction of the γ' phase; (iii) the γ/γ' misfit; (iv) TCP stability index; (v) density; and (vi) cost.

lie to the bottom of the diagram. Evidently, alloys with low cost are not necessarily the most stable, and vice versa. Cheap alloys can be either stable or unstable, as can expensive ones. This is because Re alloying is predicted to have only a weak influence on the predicted stability, as governed by its M_{di} number (see Fig. 8).

4.3. Scatter diagrams

To study the factors which influence the alloy design process further, scatter diagrams have been constructed on which the predicted characteristics are plotted against one another. Plots involving the fraction of the γ' phase (calculated at 900 °C) are particularly insightful. Consider Fig. 12a, on which the data are plotted against the density. One sees that, as the γ' content increases due to additions of Al and Ta, the alloys in general become less dense; this is a consequence of the low density of Al but also because some of the heavier elements such as Re are γ-formers, thus partitioning to γ. The data fall into four distinct regions because calculations have been made at a resolution of 1 wt.%. Interestingly, the data are less clustered at lower

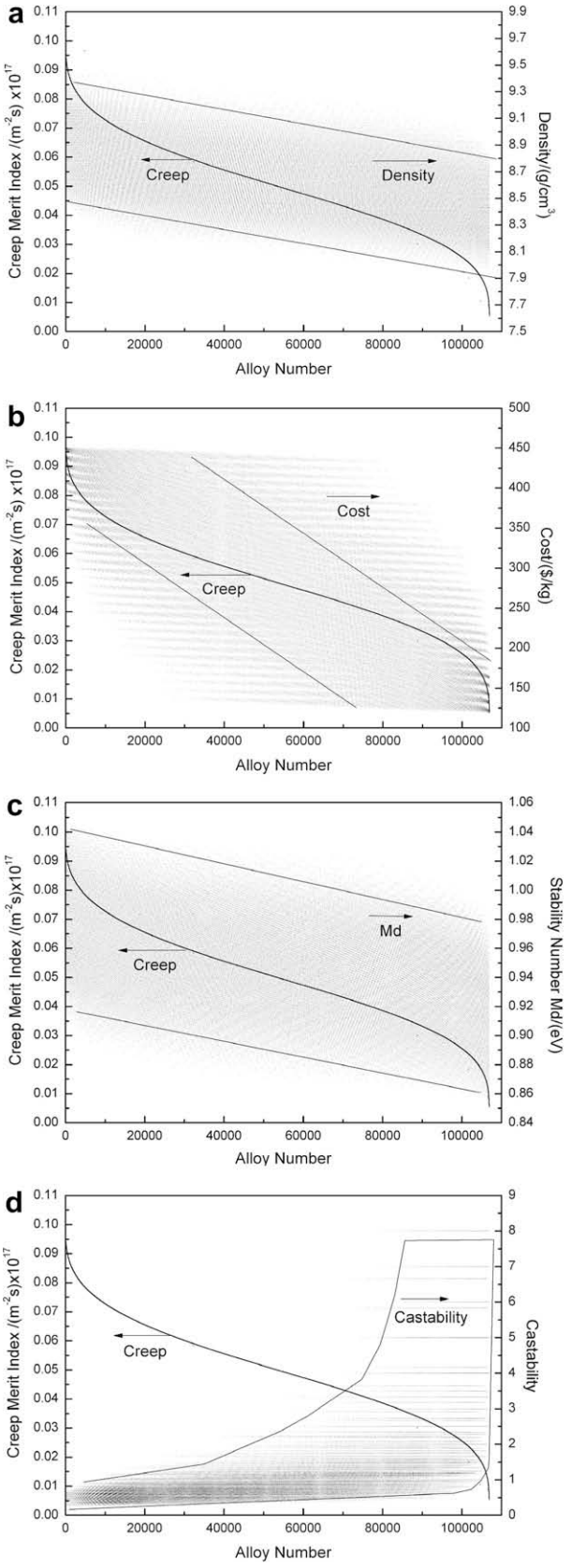

Fig. 10. Examples of trade-off diagrams: (a) creep merit index vs. density; (b) creep merit index vs. cost; (c) creep merit index vs. stability number M_d; and (d) creep merit index vs. castability.

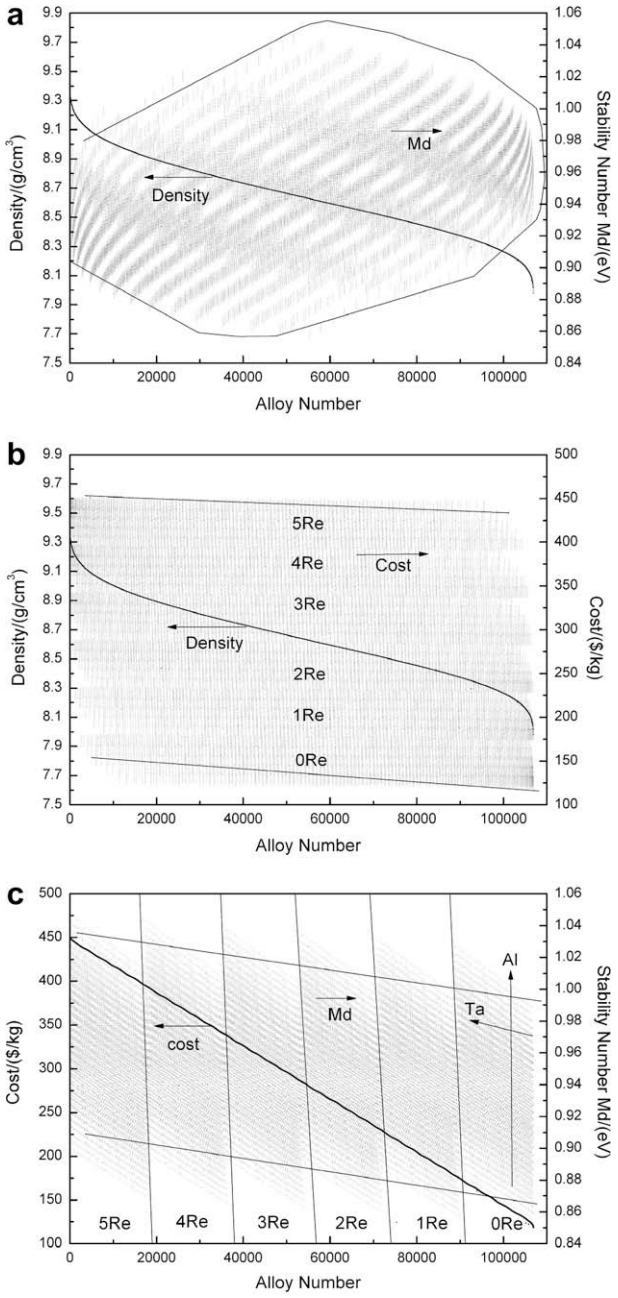

Fig. 11. Examples of trade-off diagrams: (a) density vs. stability number M_d; (b) density vs. cost; and (c) cost vs. stability number M_d.

fractions of γ'; this is because significant quantities of the γ-forming elements, such as Re and W – which impact strongly on density – are then present. Interrogation of the data has confirmed that Ta increases from bottom left to top right; it is not such a strong γ' forming element as Al. Use is made of this in Section 5.2.

The scatter plot of fraction γ' vs. cost is given in Fig. 12b. Once again, one sees the influence of the γ' forming elements Al and Ta, the former acting more strongly than the latter. However, the cost is dominated by the Re content and this allows the near-vertical lines to be drawn on the figure. The influence of Ta – the next most expensive

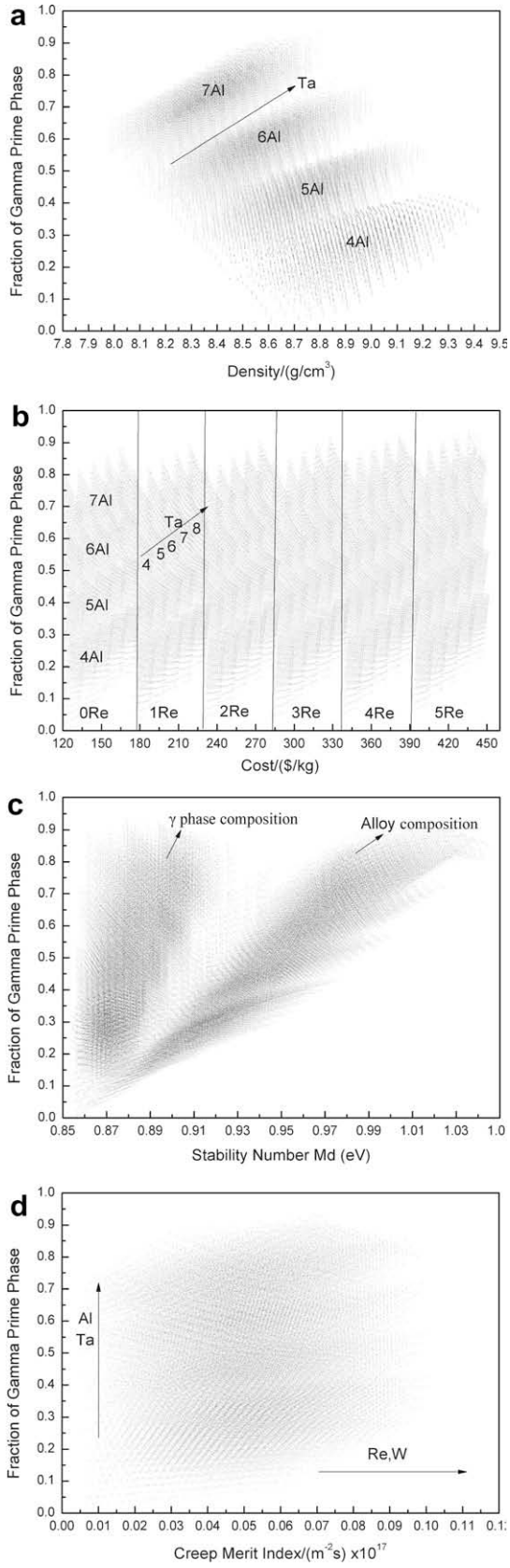

Fig. 12. Examples of scatter diagrams: (a) fraction of γ' phase vs. density; (b) fraction of γ' phase vs. cost; (c) fraction of γ' phase vs. stability number M_d; and (d) fraction of γ' phase vs. creep merit index.

element in the compositional space considered (see Fig. 4) – is less marked. Next, consider the plot against the stability number $\overline{M_d}$ (see Fig. 12c); calculations have been made using (i) the mean compositions of the alloys $\bar{x}$ and (ii) the computed fractions in the γ phase x_i^{γ}. The data fall into two distinct regions, depending upon which of (i) or (ii) is employed, with values of the stability number being greater when the mean compositions are used. Consistent with the data of Fig. 8, alloying particularly with Al and Ta has a tendency to promote instability. Finally, the scatter plot of fraction γ' vs. creep merit index is given in Fig. 12d. Detailed interrogation of the data in this plot confirms that the alloys towards the right hand side of the diagram are those rich in Re and W; consistent with Fig. 2, it is those towards the upper right-hand side of the diagram which need to be isolated, as those which are likely to perform best in creep. This is done in the section which follows.

5. Design of new grades of single crystal superalloy

The calculations presented above provide valuable insight. However, for the purposes of alloy design it has been discovered that significant power arises when bounds are placed on the values of the properties (e.g. density, cost, creep resistance, stability) which can be accepted, with the models then being applied sequentially. This allows – by the systematic application of the models to reduce the size of the alloy design space – compositions to be isolated which should be close to those which are optimal. Clearly, this is an approach which is fundamentally different from that employed traditionally, since it requires the systematic elimination of unsuitable alloys by appealing to design constraints. It is a first step towards the design of these alloys using sound physical principles. Two applications – for alloys suitable for (i) jet propulsion and (ii) land-based electricity generating turbines – are considered.

5.1. Design of an alloy system for jet propulsion

Consider the dataset of ~100,000 alloys identified in Section 4 above. Fig. 2 indicates that an optimal alloy is likely to have a fraction of the γ' phase in the range 0.60–0.70; application of this criterion reduces the size of the dataset considerably to ~16,700. All are found to have a relative density of less than 9.0. One can reduce the size of the dataset further by appropriate choice of the lattice misfit, *ie* $|\delta|$; for example, it is known that CMSX-4 – which has exceptional resistance to γ coarsening – has $\delta = +8 \times 10^{-4}$ at 900 °C [5] and one might desire to choose an alloy which exhibits a value within $\delta = \pm 2.5 \times 10^{-4}$ of this, so that $\delta = (+8 \pm 2.5) \times 10^{-4}$. Alternatively, one might decide that a small negative misfit is appropriate, so that $\delta = (-8 \pm 2.5) \times 10^{-4}$, or a misfit close to zero, so that $\delta = (0 \pm 2.5) \times 10^{-4}$. Here, these are referred to as the positive, zero and negative misfit alloys; application

of these criteria reduces the size of the dataset to 838, 2306 and 2661 alloys respectively. One can be more prescriptive. For example, if one requires an alloy of relative density less than 8.5 one is left with 443, 638 and 992 alloys respectively. Alternatively, one could require a tolerance of $M_{\mathrm{d}} < 0.9615$ so that the alloy is predicted to be more stable than CMSX-4 and CMSX-10 – in which case one has 489, 607 and 605 alloys respectively. Requiring both a density less than 8.5 and $M_{\mathrm{d}} < 0.9615$ leaves 286, 317 and 348 alloys respectively; the alloy which is predicted to have the best creep resistance is negatively misfitting and has a composition Ni–4Cr–10Co–3Re–3W–7Al–5Ta (wt.%), with a creep merit index of 5.4×10^{15} m^{-2} s.

It is of interest to examine the compositions of the alloys in these much smaller datasets. It is found that alloys with a range of Cr compositions are present, and probably this is due to the significant solubility of Cr in the Ni lattice as seen in the Ni–Cr binary phase diagram. In Fig. 13, the alloys with the best M_{creep} in the positive, zero and negatively misfitting categories above (of dataset sizes 838, 2306 and 2661 respectively) are plotted as a function of their Cr content; also plotted is a dotted line corresponding to the best M_{creep} found in the original dataset of ~16,700 alloys. Note that no criterion has been placed on either density or stability. It is predicted that the creep performance varies markedly with Cr content; this is of significance since the resistance to oxidation, corrosion and sulphidization is improved markedly at higher chromium contents; one might therefore in practice wish to maintain a minimum Cr level dependent upon the quality of the fuel used and the mission characteristics of the engine. Interestingly, for quite a wide range of Cr contents, the negatively misfitting alloys are predicted to exhibit a creep resistance close to the theoretical limit. The creep merit indices for those alloys which are predicted to perform best, as a function of both Cr and Re contents, are plotted in Fig. 14a and b for the zero and negative lattice misfitting categories respectively. Particularly at medium to high Cr contents, the negatively misfitting alloys are predicted to outperform the zero misfit ones. If one requires a relative density of 8.75 or less, then our predictions indicate that the creep

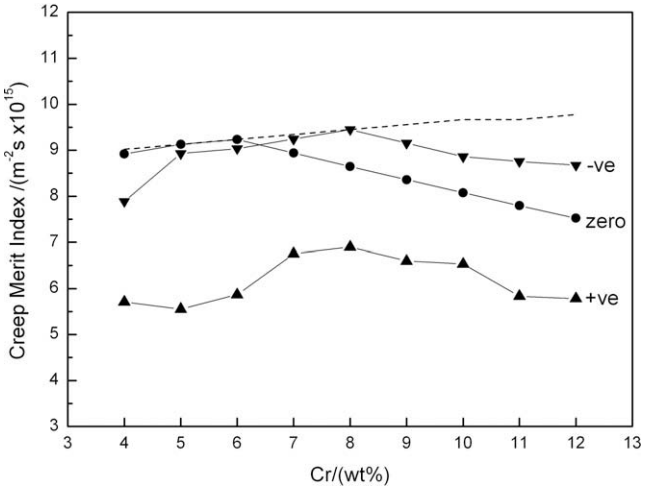

Fig. 13. Variation of the maximum predicted creep merit index M_{creep} as a function of Cr content, for optimized alloys of misfit δ equal to $(-8 \pm 2.5) \times 10^{-4}$ (negative), $\pm 2.5 \times 10^{-4}$ (zero) and $(+8 \pm 2.5) \times 10^{-4}$ (positive).

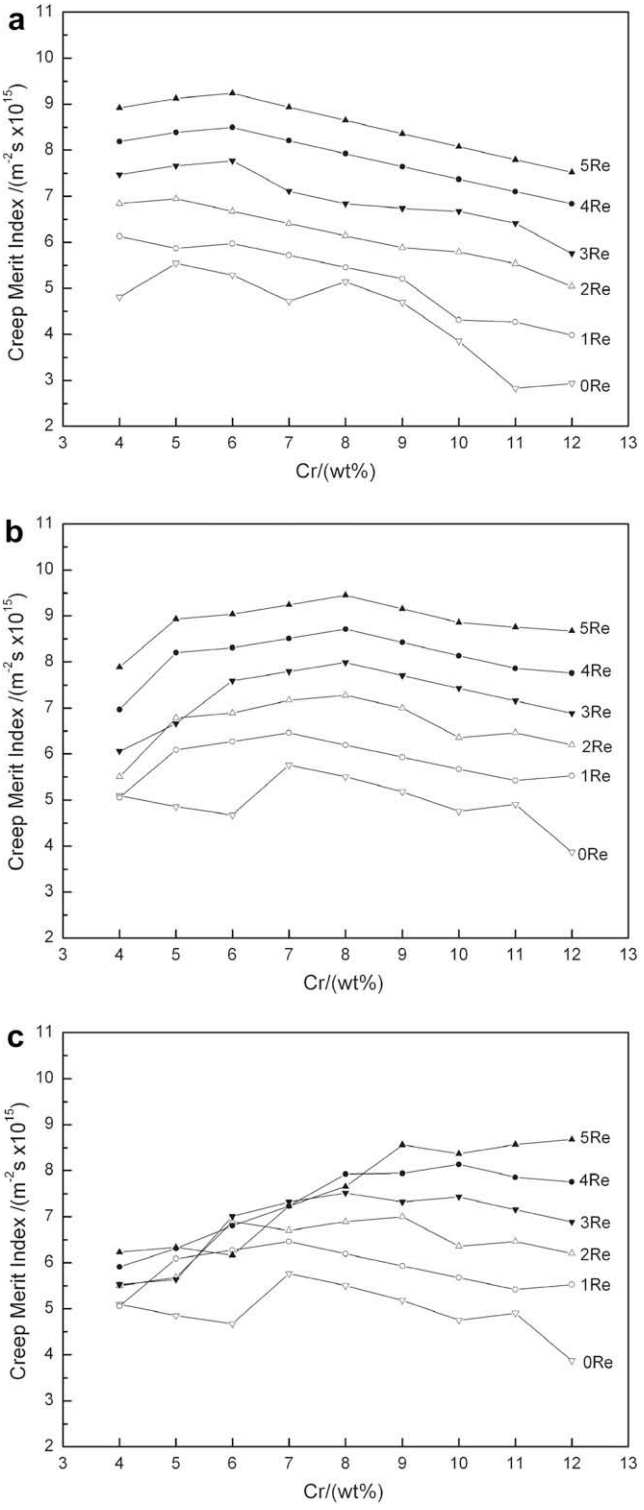

Fig. 14. Variation of the maximum predicted creep merit index M_{creep} as a function of Cr and Re contents, for (a) optimized alloys of misfit δ equal to $\pm 2.5 \times 10^{-4}$ (zero), (b) $(-8 \pm 2.5) \times 10^{-4}$ (negative) and (c) $(-8 \pm 2.5) \times 10^{-4}$ (negative), but with relative density no greater than 8.75.

performance will be compromised at the low to mid-range Cr contents (see Fig. 14c). These findings indicate that alloys with Cr contents in the range 7–9 wt.%, with negative misfit, are promising. Table 3 lists the compositions of the alloys of Fig. 14b. The composition Ni–8Cr–10Co–3Re–8W–6Al–8Ta is the alloy of Fig. 14b that is predicted to perform best in creep at the 3 wt.% Re level. Our calculations indicate that a Cr concentration of 8 wt.% is perhaps the highest that can be tolerated before significant TCP stability occurs (see Fig. 15) since for higher concentrations the predicted $\overline{M_d}$ number increases markedly.

Since the computations were carried out with 1 wt.% resolution only, one might ask whether this can be improved. To illustrate that this is indeed possible –

Table 3
Compositions of the aeroengine gas turbine alloys designed in this study.

Alloy	Cr	Co	Re	W	Al	Ta	Ni	Density (g/cm^3)
1	4	10	0	8	7	4	Bal	8.43
2	5	10	0	7	7	4	Bal	8.37
3	6	10	0	6	7	5	Bal	8.35
4	7	10	0	8	6	8	Bal	8.70
5	8	10	0	7	6	8	Bal	8.64
6	9	10	0	6	6	7	Bal	8.54
7	10	7	0	6	6	8	Bal	8.56
8	11	9	0	5	6	8	Bal	8.50
9	12	5	0	4	6	8	Bal	8.44
10	4	10	1	6	7	4	Bal	8.39
11	5	10	1	8	6	6	Bal	8.71
12	6	10	1	8	6	7	Bal	8.73
13	7	10	1	8	6	8	Bal	8.75
11	8	10	1	7	6	8	Bal	8.68
15	9	10	1	6	6	8	Bal	8.62
16	10	10	1	5	6	8	Bal	8.56
17	11	10	1	4	6	8	Bal	8.50
18	12	10	1	4	6	8	Bal	8.48
19	4	10	2	5	7	6	Bal	8.46
20	5	10	2	8	6	6	Bal	8.75
21	6	10	2	8	6	6	Bal	8.74
22	7	10	2	8	6	8	Bal	8.79
23	8	10	2	8	6	8	Bal	8.77
21	9	10	2	7	6	8	Bal	8.71
25	10	10	2	5	6	8	Bal	8.60
26	11	10	2	5	6	8	Bal	8.59
27	12	10	2	4	6	8	Bal	8.53
28	4	4	3	8	6	5	Bal	8.78
29	5	6	3	8	6	6	Bal	8.80
30	6	10	3	8	6	6	Bal	8.78
31	7	10	3	8	6	7	Bal	8.80
32	8	10	3	8	6	8	Bal	8.82
33	9	10	3	7	6	8	Bal	8.76
34	10	10	3	6	6	8	Bal	8.69
35	11	10	3	5	6	8	Bal	8.63
36	12	10	3	4	6	8	Bal	8.57
37	4	5	4	8	6	5	Bal	8.83
38	5	10	4	8	6	6	Bal	8.85
39	6	10	4	8	6	6	Bal	8.83
40	7	10	4	8	6	7	Bal	8.85
41	8	10	4	8	6	8	Bal	8.87
42	9	10	4	7	6	8	Bal	8.80
43	10	10	4	6	6	8	Bal	8.74
41	11	10	4	5	6	5	Bal	8.68
45	12	9	4	5	6	8	Bal	8.66
46	4	6	5	8	6	5	Bal	8.90
47	5	10	5	8	6	6	Bal	8.90
48	6	10	5	8	6	6	Bal	8.88
49	7	10	5	8	6	7	Bal	8.90
50	8	10	5	8	6	8	Bal	8.92
51	9	10	5	7	6	8	Bal	8.85
52	10	10	5	6	6	8	Bal	8.79
53	11	9	5	6	6	8	Bal	8.77
54	12	10	5	5	6	8	Bal	8.71

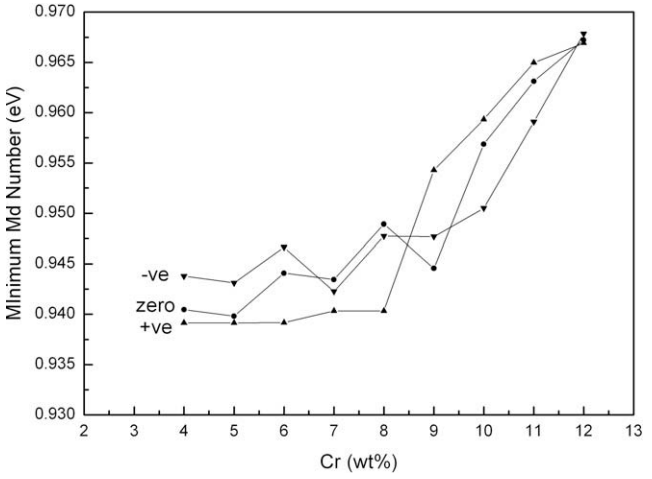

Fig. 15. Variation of the stability number M_d of the alloys predicted to be the most stable as a function of Cr content, for alloys of misfit δ equal to $(-8 \pm 2.5) \times 10^{-4}$ (negative), $\pm 2.5 \times 10^{-4}$ (zero) and $(+8 \pm 2.5) \times 10^{-4}$ (positive). No restriction is placed on density.

although at further computational cost – an additional level of optimization has been carried out. For those alloys contained in the dataset of 2661 (negatively misfitting) alloys above and implied by Fig. 13, further calculations were made at an improved resolution of 0.1 wt.% for the alloying additions Al, W, Ta and Re; this required an additional 11^4 calculations for each of the alloys in the original dataset of 2661. The completed dataset can be interrogated in various ways. For example, what is the composition of the alloy containing 3 wt.% Re that is predicted to perform the best in creep? It is found to be Ni–8Cr–10Co–3Re–8.5W–5.9Al–8.5Ta (wt.%); this alloy possesses a relative density of 8.88 and a predicted creep merit index of 8.2×10^{15} m^{-2} s. Our predictions indicate that it should perform better than CMSX-4 – the most commonly used second-generation alloy containing 3 wt.% Re – exceeding the life at 900 °C, 390 MPa by about 100 h. Further calculations are possible; for example, an alloy of composition Ni–8Cr–10Co–1.6Re–8.5W–5.8Al–8.5Ta (wt.%) (relative density of 8.83 and predicted creep merit index of 7.2×10^{15} m^{-2} s) is found to be the alloy with lowest Re content, which is predicted to match the creep performance of CMSX-4; it is cheaper by a factor of approximately 1.6/3 or 53% on account of its lower Re content. In Section 6 below, these two alloys are referred to as Alloy ABD-1 and Alloy ABD-2 respectively. The alloy Ni–8Cr–10Co–2.1Re–8.3W–6.1Al–8.2Ta (wt.%) (relative density of 8.78 and predicted creep merit index of 7.5×10^{15} m^{-2} s) has a predicted ratio of creep merit index/density that exceeds that of CMSX-4 and should offer a good combination of creep performance and cost.

5.2. Design of an alloy system for industrial gas turbines

Traditionally, single crystal superalloys have been developed for jet engines, and there have been few, if any, alloys developed specifically for the industrial gas turbines (IGTs) used for electricity generation. Therefore, there has been a tendency for the IGT community to use aerospace alloys such as CMSX-4 and Rene N5 for their applications, when in reality bespoke ones for these applications may be preferred. Thus, it is probable that greater emphasis needs to be placed on conferring greater corrosion resistance than has traditionally been required, since the fuels used for aeroengines tend to be much cleaner than those used for IGTs. Moreover, the blades are considerably larger than for the aeroengine case; therefore (i) the cost of the raw elemental additions is a substantial issue and (ii) the castability of the alloy should be maximized since it is known that freckling is enhanced as casting size increases.

Fig. 16 illustrates the alloy design problem from the industrial gas turbine perspective. Existing grades of nickel-based superalloy are plotted on a graph of Cr content vs. Al content. In the upper left-hand corner (Rene N5, PWA 1484, MC2, etc.) are examples of single crystal superalloys derived specifically for aeroengine applications; they have appreciable creep strength due to (amongst other factors) their Al content, but lack the Cr content to confer adequate corrosion resistance for IGT applications. Older alloys, such as IN792 and IN738LC, have sufficient corrosion resistance but lack strength; moreover, they are not designed to be single crystal superalloys. As indicated, there is scope for the design of new grades of single crystal superalloy for these applications, matching the Al content of the aeroengine alloys at higher Cr contents for enhanced corrosion resistance.

The methods have been used to design new grades of single crystal superalloy for IGT applications. The following criteria were applied: (i) the Re content was kept at zero, since for these applications castability should be maximized and cost minimized (whilst maintaining adequately long component lifetime); (ii) the Cr content should be appreciably higher than for the aeroengine alloys, in the range 12–20 wt.%, on account of the need for corrosion resistance; (iii) the γ' fraction was kept in the range 0.5–0.6, a little lower than for the aeroengine alloy, to maintain a good combination of creep resistance, fatigue and microstructural stability; and (iv) the lattice misfit should be in the range $\delta = (-8 \pm 2.5) \times 10^{-4}$, as before. Within these constraints, it has proven possible to find alloys which are likely to be close to optimal; these compositions are given in Table 4. In Fig. 17 the predicted creep merit index is plotted as a function of Cr content and the $\overline{M_d}$ stability index. One can see that, for a given limit of instability that can be accepted (implying a maximum tolerable $\overline{M_d}$), the creep resistance must decrease with increasing Cr content and thus corrosion resistance. Table 4 indicates that this is due to the smaller W and Co contents that are needed at high Cr concentrations. As expected, the predicted creep resistance is inferior to the aerospace alloys of Section 5.1, due to the lack of Re alloying; however, this is offset by the vastly decreased cost and greater castability of these alloys (see Section 6). Compositions close to those given in Table

Table 4
Compositions of IGT alloys designed in this study.

Alloy	Cr	Co	W	Al	Ta	Ni	Density (g/cm^3)
$\overline{M_d} < 1.000$							
Alloy 55	12	10	7	5.2	8.0	Bal	8.71
Alloy 56	13	10	7	5.0	8.0	Bal	8.73
Alloy 57	14	10	5	5.4	8.0	Bal	8.55
Alloy 58	15	10	5	5.2	8.0	Bal	8.57
Alloy 59	16	9	3	5.4	8.0	Bal	8.43
Alloy 60	17	10	3	5.4	8.0	Bal	8.41
Alloy 61	18	10	4	5.2	8.0	Bal	8.47
Alloy 62	19	7	4	5.2	8.0	Bal	8.45
Alloy 63	20	10	4	5.0	8.0	Bal	8.47
$\overline{M_d} < 0.985$							
Alloy 64	12	10	7	5.2	8.0	Bal	8.71
Alloy 65	13	10	7	5.0	8.0	Bal	8.73
Alloy 66	14	10	5	5.4	7.8	Bal	8.54
Alloy 67	15	10	4	5.4	7.8	Bal	8.57
Alloy 68	16	9	3	5.4	8.0	Bal	8.43
Alloy 69	17	4	3	5.4	7.8	Bal	8.25
Alloy 70	18	4	1	5.8	7.2	Bal	8.30
Alloy 71	19	1	0	5.8	7.4	Bal	8.27
$\overline{M_d} < 0.975$							
Alloy 72	12	10	7	5.2	7.0	Bal	8.67
Alloy 73	13	10	5	5.4	7.0	Bal	8.53
Alloy 74	14	9	4	5.6	6.6	Bal	8.42
Alloy 75	15	10	1	6.0	6.6	Bal	8.22
Alloy 76	16	3	1	6.0	6.6	Bal	8.20
Alloy 77	17	1	0	6.0	6.8	Bal	8.15
$\overline{M_d} < 0.962$							
Alloy 78	12	10	3	6.0	5.0	Bal	8.29
Alloy 79	13	7	2	6.0	5.4	Bal	8.25
Alloy 80	14	4	1	6.0	5.4	Bal	8.19
Alloy 81	15	1	0	6.0	5.8	Bal	8.15

4 are now being evaluated experimentally [32]. The alloy of composition Ni–15Cr–10Co–4W–5.5Al–7.8Ta (wt.%) is referred to as Alloy ABD-3 in Section 6.

6. Discussion – improved castability index

Fig. 10d implies a strong trade-off between creep resistance and the freckling susceptibility, on which the castability was assumed to depend. However, in Section 4 only a first-order approximation was made for freckling; a more sophisticated analysis is desirable given the need to ensure ease of processing of these materials. Frequently, a non-dimensional mushy zone Rayleigh number (Ra) has been invoked to explain the important aspects of the freckling phenomenon. Whilst a number of different versions have been proposed (e.g. [20,21,29,30]), a common feature is a definition dependent upon the ratio of the driving buoyancy force to the retarding frictional force associated with the permeability of the semi-solid region. Thus, for example, one has [21]

$$\mathrm{Ra}_h = \frac{(\Delta\rho/\rho_o) g \overline{K} h}{\alpha \nu} \tag{9}$$

where the subscript h on the Rayleigh parameter Ra refers to the height within the semi-solid zone, which varies from

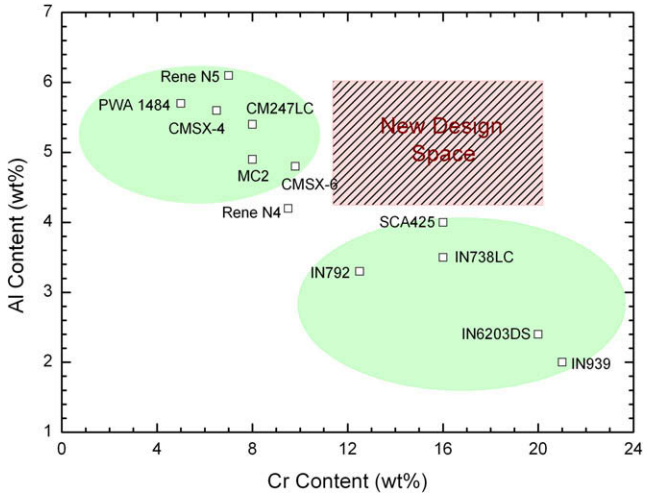

Fig. 16. Illustration of the proposed design space for IGT alloys.

0 at the liquidus to a maximum H at the solidus. The term $\Delta\rho/\rho_o$ is the relative liquid density inversion at height h, consistent with

$$\Delta\rho/\rho_o = (\rho_o - \rho\{h\})/\rho_o \tag{10}$$

where ρ_o is the liquid density at the liquidus and $\rho\{h\}$ is the density evaluated at height h. Other terms in Eq. (9) include the acceleration due to gravity g, the mean permeability of the semi-solid $\overline{K}$, the thermal diffusivity α and the kinematic viscosity ν.

For the purposes of the present work, it will be assumed that the single crystal superalloys can be ranked for their susceptibility to freckling by estimating the relative liquid density inversion, $\Delta\rho/\rho_o$, at a value of h corresponding to 0.10 fraction solid. Thus, it is assumed that the other terms in Eq. (9) do not, to a first-order approximation, have a strong dependence upon chemical composition. This assumption is supported by the finding [21] that the same critical Rayleigh number applies to different superalloys, and our calculations which confirm that parameters associated with the resistive terms of Eq. (9) (particularly $\overline{K}$) depend more strongly upon processing conditions than alloy chemistry. Our estimates are made as follows. Use is made of the careful experimental work of Mills et al [31], which has confirmed that the density of liquid CMSX-4 at the melting point is 7.754 g cm^{-3}, varying by an amount -0.0009 g cm^{-3} K^{-1} with temperature in a linear fashion. These data, along with the predicted equilibrium partitioning of solutes during solidification, allow the density of the liquid in the semi-solid region to be estimated for CMSX-4 (see Fig. 18). The dotted line represents an extrapolation of the liquid density below the liquidus, based upon the experimental data [31]; in the semi-solid region, the density of the liquid is reduced due to the partitioning of elements such as Re and W to the solid phase. The form of the curve below the liquidus represents a rationalization of the susceptibility of these alloys to freckling. Note that the relative change in density has been calculated on the basis of atomic weights only; no account has been taken of changes in specific molar volumes or second-order solute interac-

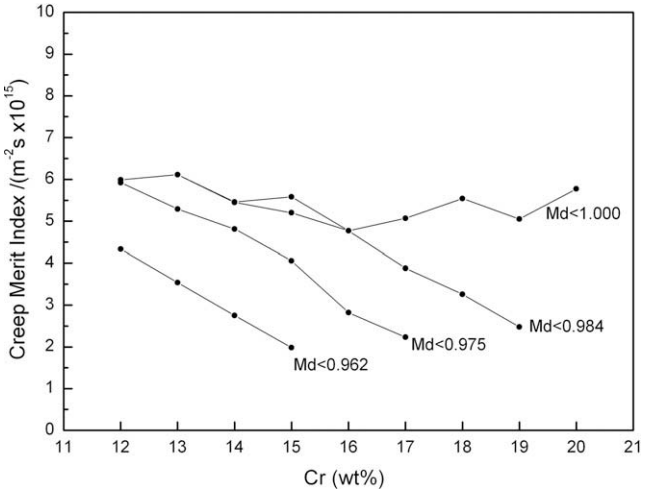

Fig. 17. Variation of maximum predicted creep merit index M_{creep} as a function of Cr content, for alloys with various values of the stability index $\overline{M_d}$.

tions. Thus, in order to estimate the reduction in the liquid density in the semi-solid region, the value from the dotted line of Fig. 18 (at which the solid fraction equals 0.10) is scaled by a factor $\sum_i x_i^L m_i / \sum_i \bar{x}_i m_i$ where the m_i are the atomic weights and x_i^L and $\bar{x}_i$ correspond to the mole fractions of i in the partitioned liquid and the mean mole fraction respectively. Estimates made in a similar way, again making use of the experimental data for CMSX-4 and scaling it appropriately, are also given in Fig. 17 for the first-generation single crystal superalloy Rene N4 and the third-generation single crystal superalloy CMSX-10. One can see that the relative liquid density inversion, $\Delta\rho/\rho_o$, will be larger for the freckle-prone CMSX-10. Note the larger and smaller densities of CMSX-10 and Rene N4 respectively compared to CMSX-4, consistent with the density data of Table 1.

These methods can be used for the ranking of the both existing and proposed alloys for their susceptibility to freckling. To do this, the quantity $\Delta\rho/\rho_o$ is calculated with the liquid density ρ_o estimated at the melting point and the density $\rho\{h\}$ (required for the estimate of $\Delta\rho$) evaluated at a constant fraction solid of 0.10. Again, use is made of the Thermocalc software for these calculations. In Table 5, values for the relative liquid density inversion, $\Delta\rho/\rho_o$, are given for the important single crystal superalloys of Table 1. The ranking of the alloys calculated has been found to be rather insensitive to the fraction solid assumed for $\rho\{h\}$. Consistent with foundry experience, the third-generation single crystal alloys such as CMSX-10 and Rene N6 are predicted to be the most prone to freckling due to their large and negative values of $\Delta\rho/\rho_o$, which promote freckle plumes. The values for the proposed alloys ABD-1, ABD-2 and ABD-3 are large and positive, so that the buoyancy forces forces for these alloys act in the same direction as the gravity vector, rather than against it. This is likely to mean that the castability is favourable, although experimental confirmation of this is needed.

Table 5
Predictions for the castability of the new alloys ABD-1, ABD-2 and ABD-3 in comparison with existing single crystal superalloys.

Alloy	$\Delta\rho/\rho_0$
ABD-3	**−0.00266**
PWA 1480	−0.00219
ABD-2	**−0.00109**
AM1	-0,000839
ABD-1	**−0.000829**
CMSX-6	−0.000552
PWA 1484	−0.000420
Rene N5	-6.00×10^{-6}
MC2	-4.08×10^{-6}
MX4	0.000141
TMS-6	0.000193
CMSX-4	0.000205
Rene N4	0.000296
RR2000	0.000310
AM3	0.000450
TMS-82+	0.000532
Rene N6	0.000662
CMSX-2	0.00105
TMS-75	0.00134
SRR99	0.00142
TMS-12	0.00148
Nasair 100	0.00170
TMS-162	0.00171
TMS-138	0.00228
MC-NG	0.00252
CMSX-10	0.00278

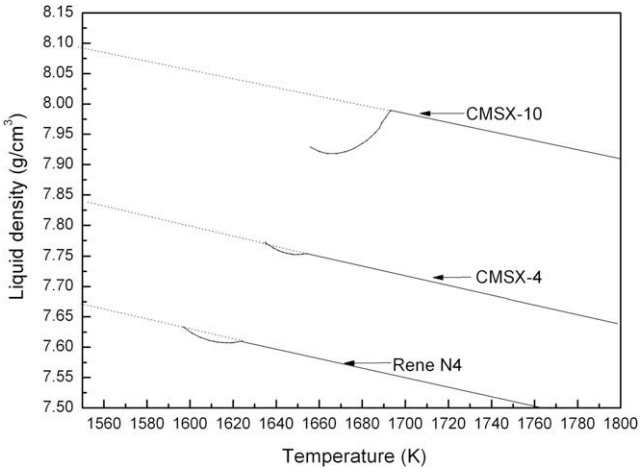

Fig. 18. Predictions of the variation of the density of the liquid phase for the alloys CMSX-10, CMSX-4 and Rene N4 as a function of temperature and during solidification. The point of deviation from the straight line in each case occurs at the melting point; at lower temperatures the density of the unpartitioned liquid is estimated by extrapolation, with the solid line corresponding to the density of the remaining liquid after partitioning of solutes (specifically Re, W and Ta) is accounted for.

7. Conclusions

The following conclusions can be drawn from this work:

1. Procedures have been developed which allow the compositions of single crystal superalloys to be designed by appealing to numerical estimates of creep resistance, microstructural stability, density, cost and castability.

2. The approach involves the cycling over a wide compositional space, eliminating from it those alloys which are deemed to be unsuitable on the basis of design criteria and predictions from models which are entirely physically based.
3. Calculations indicate that a number of trade-offs exist in these systems. For example, castability and cost are compromised when the very best creep resistance is required; those performing best in creep are those which are the most dense. The modelling allows these trade-offs to be studied quantitatively.
4. Application of the procedures has allowed a number of prototype alloys to be identified. These are suitable for future testing, to confirm their properties. We believe these to be the first single crystal superalloys designed upon purely theoretical grounds.
5. This new approach contrasts strongly with that used traditionally, which has involved the identification of just a few alloys based upon prior experience, and the ranking of them by subsequent testing.
6. The alloy design procedures proposed can obviously be improved upon as more accurate models (e.g. for creep resistance, TCP susceptibility) become available.

Acknowledgements

R.C.R. and N.W. acknowledge a grant (EP/D047048/1) "Alloys by Design: A Materials Modelling Approach" from the Engineering and Physical Sciences Research Council (EPSRC) of the United Kingdom, which has been used to fund this work. Discussions over many years with Dr Cathie Rae (University of Cambridge), Dr Bob Broomfield (University of Birmingham), Dr Robbie Hobbs (Rolls-Royce plc) and Dr Magnus Hasselqvist (Siemens Industrial Turbomachinery) are acknowledged. Professor John Knott (University of Birmingham) made some helpful comments on an early version of the manuscript, for which the authors are grateful.

References

[1] Reed RC, Green KA, Caron P, Gabb TP, Fahrmann MG, Huron ES, et al., editors. Superalloys 2008. Warrendale (PA): TMS; 2008.
[2] McLean M. Phil Trans Royal Soc London A 1995;351:419–33.
[3] Reed RC. Superalloys: fundamentals and applications. Cambridge: Cambridge University Press; 2006.
[4] Harris K, Erickson GL, Sikkenga SL, Brentnall WD, Aurrecoechea JM, Kubarych KG. In: Antolovich SD, Stusrud RW, MacKay RA, Anton DL, Khan T, Kissinger RD, et al., editors. Superalloys 1992. Warrendale (PA): The Minerals, Metals and Materials Society; 1992. p. 297–306.
[5] Harada H, Murakami H. In: Saito T, editor. Computational materials design. Berlin: Springer-Verlag; 1999. p. 39–70.
[6] Caron Pierre. In: Pollock TM, Kissinger RD, Bowman RR, Green KA, McLean M, Olson SL, et al., editors. Superalloys 2000. Warrendale (PA): TMS; 2000. p. 737–46.
[7] Walston S, Cetel A, Mackay R, O'Hara K, Duhl D, Dreshfield R. In: Green KA, Pollock TM, Harada H, Howson TE, Reed RC, Schirra JJ, et al., editors. Superalloys 2004. Warrendale (PA): TMS; 2004. p. 15–24.
[8] Koizumi Y, Kobayashi T, Yokokawa T, Zhang J, Osawa M, Harada H, et al. In: Green KA, Pollock TM, Harada H, Howson TE, Reed RC, Schirra JJ, et al., editors. Superalloys 2004. Warrendale (PA): TMS; 2004. p. 35–43.
[9] Cumpsty NA. Jet propulsion: a simple guide to the aerodynamic and thermodynamic design and performance of jet engines. Cambridge: Cambridge University Press; 1997.
[10] Pollock TM, Argon AS. Acta Metall Mater 1992;40:1–30.
[11] Pollock TM, Field RD. In: Nabarro FRN, Duesbery MS, editors. Dislocations in solids, vol. 11. Amsterdam: Elsevier; 2002. p. 593–5.
[12] Dyson BF. Mater Sci Technol 2009;25:213–20.
[13] Ma A, Reed RC, Dye D. Acta Mater 2008;56:1657–70.
[14] Murakumo T, Kobayashi T, Koizumi Y, Harada H. Acta Mater 2004;52:3737–44.
[15] Kuhn HA, Biermann H, Ungar T, Mughrabi H. Acta Metall Mater 1991;11:2783–94.
[16] Rae CMF, Reed RC. Acta Mater 2001;49:4113–25.
[17] Darolia R, Lahrman DF, Field RD. In: Reichman S, Duhl DN, Maurer G, Antolovich S, Lund C, editors. Superalloys 1988. Warrendale (PA): TMS; 1988. p. 255–64.
[18] Boesch WJ, Slaney JS. Metal Progress 1964;86:109–11.
[19] Murata Y, Miyazaki S, Morinaga M, Hashizume R. In: Kissinger RD, Deye DJ, Anton DL, Cetel AD, Nathal MV, Pollock TM, et al., editors. Superalloys 1996. Warrendale (PA): TMS; 1996. p. 61–70.
[20] Tin S, Pollock TM. Metall Mater Trans 2003;34A:1953–67.
[21] Beckermann C, Gu JP, Boettinger WJ. Metall Mater Trans 2000;31:2545–57.
[22] Janotti A, Krcmar M, Fu CL, Reed RC. Phys Rev Lett 2004;92:085901.
[23] Karunaratne MSA, Reed RC. Acta Mater 2003;51:2905–19.
[24] Kobayashi T, Harada H, Osawa M, Sato A. J Jpn Inst Metals 2005;69:707–10.
[25] Koizumi Y, Kobayashi T, Yokokawa T, Harada H, Aoki Y, Araki M, et al. J Gas Turbine Soc Jpn 2001.
[26] Koizumi Y, Kobayashi T, Yokokawa T, Osawa M, Harada H, Aoki Y, et al. J Jpn Inst Metals 2004;68(3):206–9.
[27] Sundman B, Agren J. J Phys Chem Solids 1981;42:297–301.
[28] Saunders N. In: Kissinger RD, Deye DJ, Anton DL, Cetel AD, Nathal MV, Pollock TM, et al., editors. Superalloys 1996. Warrendale (PA): TMS; 1996. p. 101–9.
[29] Hobbs RA, Tin S, Rae CMF. Metall Mater Trans 2005;36A:2761–75.
[30] Aubertin P, Wang T, Cockcroft SL, Mitchell A. Metall Mater Trans 2000;31B:801–11.
[31] Mills KC. Recommended values of thermophysical properties for selected commercial alloys. Materials Park (OH): ASM International; 2001.
[32] Sato A, Hasselqvist M, Moverare J, Reed RC. unpublished work.